Signal Processing 90 (2010) 809–820

Contents lists available at ScienceDirect

Signal Processing

journal homepage: www.elsevier.com/locate/sigpro

# Unitary-JAFE algorithm for joint angle–frequency estimation based on Frame–Newton method

Fulai Liu *, Jinkuan Wang, Ruiyan Du

*Engineering Optimization and Smart Antenna Institute, Northeastern University at Qinhuangdao, China*

ARTICLE INFO

*Article history:*
Received 12 February 2009
Received in revised form
24 August 2009
Accepted 28 August 2009
Available online 6 September 2009

*Keywords:*
Array signal processing
Joint angle–frequency estimation
Unitary transformation
Eigenvalue decomposition

ABSTRACT

The joint angle–frequency estimation (JAFE) based on the multidimensional ESPRIT is recently developed high-resolution parameter estimation technique for determining the directions of arrival (DOAs) and center frequencies of a number of narrow-band sources in a band of interest impinging on the far field of a planar array. In this paper, we present a simple and efficient joint angle–frequency estimation method via the unitary transformation, named as Unitary-JAFE algorithm. In the final stage of Unitary-JAFE, the matrix required to eigendecomposition is a complex unsymmetric matrix. For the eigendecomposition of a complex unsymmetric matrix, we will develop an effective algorithm based on Frame method and Newton iteration method, referred as Frame–Newton algorithm. The proposed method offers a number of advantages over other recently proposed ESPRIT-based techniques by taking advantage of the temporal smoothing, spatial smoothing, and forward–backward averaging techniques. Firstly, except for the final eigenvalue decomposition of dimension equal to the number of sources, it is efficiently formulated in terms of real-valued computation throughout. Secondly, in the final stage of the proposed algorithm, the real and imaginary parts of the $i$ th eigenvalue of a matrix are one-to-one related to the frequency and direction of arrival (DOA) of the $i$ th source. That is, the pairing of the estimated frequency and DOA is automatically determined. Thirdly, the proposed method avoids the joint diagonalization processing, which reduces the computation complexity. Finally, simulation results are presented verifying the efficacy of the proposed algorithm.



## 1. Introduction

The recovery of signal parameters from noisy observations is a fundamental problem in array signal processing. Optimal techniques based on maximum likelihood [1,2] are often applicable but might be computationally prohibitive. To reduce the complexity, Fleury et al. [3] proposed a space-alternating generalized expectation maximization (SAGE)-based algorithm, in which only a subset of the parameters is estimated iteratively while the other parameters remain fixed. Despite its effectiveness, it needs the signature of the transmit signal to achieve the signal decomposition in the expectation (E) step, and the computational load may still be too high due to the iteration process. Algebraic techniques based on a batch of data have an edge in terms of computational complexity. Such techniques make specific use of certain algebraic structures present in the data matrix. For example, a two-dimensional (2-D) multiple signal classification (MUSIC) [4]-based algorithm was considered in [5]. However, it estimates the parameters by carrying out high-dimensional eigendecompositions of the signal covariance matrices. In addition, it requires a 2-D search on the DOA-frequency plane, and thus still calls for an enormous amount of computations. To alleviate the computational overhead, several one-dimensional (1-D) subspace-based algorithms were reported. For example, Lin et al. [6] proposed FSF MUSIC which describes a tree-structured frequency-space-frequency (FSF) MUSIC-based algorithm for joint angle

* Corresponding author. Tel.: +86 335 8066033; fax: +86 335 8051795.
*E-mail address:* fulailiu@126.com (F. Liu).

0165-1684/$ - see front matter © 2009 Elsevier B.V. All rights reserved.
doi:10.1016/j.sigpro.2009.08.013

and frequency estimation. Although, with such a tree-structured estimation scheme, the estimated angles and frequencies are automatically paired without extra processing, this method employs three 1-D MUSIC-type algorithms, i.e. two F-MUSICs and one S-MUSIC. Thus, this method requires multiple 1-D search, which is computationally not very attractive, too. Another prime example of an algebraic technique is the ESPRIT algorithm [7]. Due to its simplicity and high-resolution capability, ESPRIT has been used for joint azimuth and elevation angle estimation (2-D DOA estimation) [8–11], joint DOA and delay estimation [12–14], joint angle–frequency estimation (JAFE) [15–20], etc. Their parameter estimates are obtained by exploiting the rotational invariance structure of the signal subspace, induced by the translational invariance structure of the associated sensor array. This can be achieved without computation or search of any spectral measure. In particular, Zoltowski et al. [15] discussed a similar problem of angle–frequency estimation using multiple scales in time and space. Because of ambitious goals, however, their solutions are very much directed by engineering considerations, which incur a certain sacrifice in elegance and clarity. Haardt et al. [16] discussed the problem in the context of mobile communications for space division multiple access (SDMA) applications. Their method is based on unitary-ESPRIT, which involves a certain Cayley transformation of the data to real-valued matrices. This provided a computationally efficient solution scheme but might lead to numerical inaccuracies, particularly when the eigenvalues are closed to $\pm\pi$. Chen et al. [17] made use of two 1-D estimation of signal parameters via ESPRIT algorithm to estimate these two parameter pairing with a marked subspace scheme to overcome the parameter pairing problem. This method, however, cannot discriminate the rays with very close DOAs or very close frequencies. Another 1-D ESPRIT-based algorithm was also suggested in [18], which, nevertheless, requires a special array configuration. Yet another 1-D ESPRIT-based algorithm, termed C-JAFE, was addressed recently in [19,20]. C-JAFE algorithm achieves more accurate results than previous ESPRIT-based techniques by taking advantage of the temporal smoothing, spatial smoothing, and forward–backward averaging techniques. When two or more signals have the same DOA, the array steering vectors corresponding to signals with the same DOAs are identical, and therefore, the data matrix is rank deficient. Under a certain condition, the temporal smoothing can restore the rank of the data matrix by stacking $m$ temporally shifted versions of the original data matrix. This is because the temporal smoothing enriches the structure of the array steering matrix which is referred to as the extended array steering matrix, such that the extended array steering matrix has a double Vandermonde structure. Employing a similar technique in the spatial domain, coherent signals can be separated by the spatial smoothing. Despite its high-resolution capability, the C-JAFE still involves the joint diagonalization processing apart from the singular value decomposition (SVD) or eigenvalue decomposition (EVD). That is, the C-JAFE algorithm needs to find a nonsingular matrix $\mathbf{T}$ such that $\mathbf{E}_\phi$ (which includes the information of the frequencies of incident signal sources) and $\mathbf{E}_\theta$ (which includes the information of the DOAs of incident signal sources) are simultaneously diagonalizable by the same matrix $\mathbf{T}$. It is well-known that the joint diagonalization processing is a complex nonlinear optimization procedure. If $\mathbf{E}_\phi$ and $\mathbf{E}_\theta$ are $n\times n$ real-valued matrices, the complexity of the joint diagonalization is $\mathcal{O}(n^4)$, namely, the computational complexity of the joint diagonalization is extremely demanding. Another drawback of the C-JAFE algorithm based on the joint diagonalization processing is that it needs an extra pairing procedure to match the separately estimated DOAs and frequencies. The parameter matching makes the joint angle–frequency estimation more difficult to solve.

The objective of the paper is to give a more accuracy and high resolution algorithm for the joint angle–frequency estimation, referred as Unitary-JAFE algorithm. In the final stage of Unitary-JAFE, the $i$ th eigenvalue of a matrix is the form $\tan(v_i/2)+j\tan(u_i/2)$, where $v_i=2\pi f_i/P$ and $u_i=(2\pi f_i/c)d\sin\theta_i$. $f_i$, and $\theta_i$ denote the frequency and DOA of the $i$ th source, respectively. $c$ is the speed of propagation. $d$ is the spacing between the sensors of a uniform linear array (ULA). $P$ is the sample rate. The eigenvalue for each source is thus unique such that Unitary-JAFE provides the real and imaginary parts of the $i$ th eigenvalue of a matrix are one-to-one related to $u_i$ and $v_i$, respectively. That is, the paring of the estimated frequency and DOA is automatically determined, in the final stage of new algorithm. Unitary-JAFE is developed as an extension of the C-JAFE and unitary ESPRIT [21] for a ULA. It is similar to [22]. Except for the final EVD of dimension equal to the number of sources, it is efficiently formulated in terms of real-valued computation throughout. However, the data model is different, which in turn results in different temporal and spatial signal structures. In addition, since the parameter to be estimated is now angle and frequency instead of 2-D DOA, the array steering matrix is not the same either.

The outline of this paper is organized as follows. Section 2 briefly introduces the data model and C-JAFE algorithm for joint angle–frequency estimation. In Section 3, we firstly develop the Unitary-JAFE algorithm. Secondly, the Frame–Newton method is given for solving the EVD problem of the complex unsymmetric matrix in the final stage of the Unitary-JAFE algorithm. Finally, the complexity of the proposed algorithm is addressed as well. Section 4 presents several simulation results to verify the performance of the proposed approach. Section 5 provides a concluding remark to summarize the paper.

## 2. Data model and C-JAFE algorithm

In this section, we firstly introduce the data model for the joint angle–frequency estimation. Secondly, a generalized data model is derived by the temporal smoothing and spatial smoothing processing. Finally, we review a brief development of C-JAFE algorithm for the joint angle and frequency estimation.

### 2.1. Data model

Consider a ULA of $M$ elements equispaced by $d$. Employing the center of the ULA as the phase reference, the array manifold is conjugate centrosymmetric. For example, if the

number of elements comprising the ULA $M$ is odd, there is a sensor located at the array center and the array manifold is

$$\mathbf{a}_M(f,\mu)=[e^{-j((M-1)/2)\mu},\ldots,e^{-j\mu},1,e^{j\mu},\ldots,e^{j((M-1)/2)\mu}]^T \quad (1)$$

where $\mu=(2\pi f/c)d\sin\theta$ with $f$ and $\theta$ being equal to the frequency and DOA, respectively. $c$ is the speed of propagation. $d$ is equal to the interelement spacing.

Suppose that there are $q$ narrowband sources of interest, with complex baseband representations $s_i(t)$, for $i=1,\ldots,q$. Suppose that the $i$ th source has a carrier frequency of $f_i$. The signal received at the $k$ th antenna is [19]

$$x_k(t)=\sum_{i=1}^{q}a_k(\theta_i)e^{j2\pi f_i t}s_i(t)+w_k(t)$$

where $a_k(\theta_i)$ is the antenna response of the $k$ th antenna to signal from direction $\theta_i$. $w_k(t)$ denotes the output and the additive noise of the $k$ th sensor. The observed signals at the ULA are given by

$$\boldsymbol{x}(t)=\boldsymbol{A}s(t)+\boldsymbol{w}(t) \quad (2)$$

The matrices and vectors in (2) have the following forms:

$$\boldsymbol{x}(t)=[x_1(t),x_2(t),\ldots,x_M(t)]^T\boldsymbol{A}=[\boldsymbol{a}(f_1,\mu_1),\ldots,\boldsymbol{a}(f_q,\mu_q)]$$

$$\boldsymbol{s}(t)=[s_1(t),\ldots,s_q(t)]^T\boldsymbol{w}(t)=[w_1(t),\ldots,w_M(t)]^T$$

where $x_k(t)$ and $w_k(t)$ $(k=1,\ldots,M)$ denote the output and the additive noise of the $k$ th sensor, respectively. $\boldsymbol{a}(f_k,\mu_k)$ $(k=1,\ldots,q)$ is the steering vector for the $k$ th source, which is defined by (1). The superscript $(\cdot)^T$ represents the transpose operation. Assume that $w_k(t)$ is a complex Gaussian random process with zero-mean and equal variance $\sigma^2$. The noise $w_k(t)$ is uncorrelated with $s_i(t)$.

Under the above assumptions, it can be easily seen that

$$E\{\boldsymbol{w}(t)\boldsymbol{w}^H(t)\}=\sigma^2\boldsymbol{I}$$

where $E\{\cdot\}$ represents the statistical average operation and the superscript $(\cdot)^H$ denotes the Hermitian operation.

Assume $P$ is the sample rate, which is much higher than the data rate of each source. The data sample at the receiver is

$$\mathbf{x}\left(\frac{n}{P}\right)=\sum_{i=1}^{q}\mathbf{a}(\theta_i)e^{j(2\pi/P)f_i n}s_i\left(\frac{n}{P}\right)+\mathbf{w}\left(\frac{n}{P}\right)$$

In matrix form, this can be written as

$$\mathbf{x}\left(\frac{n}{P}\right)=\mathbf{A}\boldsymbol{\Phi}^n\mathbf{s}\left(\frac{n}{P}\right)+\mathbf{w}\left(\frac{n}{P}\right)$$

where $\boldsymbol{\Phi}=\mathrm{diag}\{[\phi_1,\ldots,\phi_q]\}$ with $\phi_i=e^{j(2\pi/P)f_i}$ for $i=1,\ldots,q$, which includes the information of the frequencies of incident signal sources, e.g., we refer to matrix $\boldsymbol{\Phi}$ as time factor matrix and its diagonal element as time factor. Assume that we have collected $N$ samples of the array output $\mathbf{x}(t)$ at a rate $P$ into the $M\times N$ data matrix, ie.,

$$\mathbf{X}=\mathbf{A}\left[\mathbf{s}(0),\boldsymbol{\Phi}\mathbf{s}\left(\frac{1}{P}\right),\ldots,\boldsymbol{\Phi}^{N-1}\mathbf{s}\left(\frac{N-1}{P}\right)\right]+\mathbf{W}\in\mathcal{C}^{M,N}$$

where $\mathbf{W}\in\mathcal{C}^{M,N}$ is a matrix collecting $N$ samples of the $M\times 1$ array noise vector.

### 2.1.1. Temporal smoothing

In this subsection, we consider a data stacking technique, which is referred as temporal smoothing. An $m$-factor temporal smoothed data matrix is constructed by stacking $m$ temporally shifted versions of the original data matrix. Assume that $m=2n+1$ is odd. This results in the following $mM\times(N-m+1)$ matrix [19]:

$$\mathbf{X}_m=\begin{bmatrix}\mathbf{A}\left[\mathbf{s}(0)\boldsymbol{\Phi}\mathbf{s}\left(\frac{1}{P}\right)\cdots\boldsymbol{\Phi}^{N-m}\mathbf{s}\left(\frac{N-m}{P}\right)\right]\\ \mathbf{A}\boldsymbol{\Phi}\left[\mathbf{s}\left(\frac{1}{P}\right)\boldsymbol{\Phi}\mathbf{s}\left(\frac{2}{P}\right)\cdots\right]\\ \vdots\\ \mathbf{A}\boldsymbol{\Phi}^{m-1}\left[\mathbf{s}\left(\frac{m-1}{P}\right)\boldsymbol{\Phi}\mathbf{s}\left(\frac{m}{P}\right)\cdots\right]\end{bmatrix}+\mathbf{W}_m \quad (3)$$

where $\mathbf{W}_m$ represents the noise term constructed from $\mathbf{W}$ in a similar way as $\mathbf{X}_m$ is obtained from $\mathbf{X}$. Assume that the signals are narrow band, i.e., $s(t)\approx s(t+1/P)\approx\cdots\approx s(t+(m-1)/P)$. In this case, all the block rows in the right-hand term of (3) are approximately equal, which means that $\mathbf{X}_m$ has the following factorization:

$$\mathbf{X}_m\approx\begin{bmatrix}\mathbf{A}\boldsymbol{\Phi}^{-n}\\ \vdots\\ \mathbf{A}\boldsymbol{\Phi}^{-1}\\ \mathbf{A}\\ \mathbf{A}\boldsymbol{\Phi}\\ \vdots\\ \mathbf{A}\boldsymbol{\Phi}^{n}\end{bmatrix}\left[\boldsymbol{\Phi}^n\mathbf{s}\left(\frac{n}{P}\right)\cdots\boldsymbol{\Phi}^{N-n-1}\mathbf{s}\left(\frac{N-n-1}{P}\right)\right]+\mathbf{W}_m$$

$$\triangleq\mathbf{A}_m\mathbf{F}_s+\mathbf{W}_m\in\mathcal{C}^{mM,N-m+1}$$

where $\mathbf{A}_m$, throughout the sequel, which is referred to as the extended array steering matrix, is given by

$$\mathbf{A}_m=\begin{bmatrix}\mathbf{A}\boldsymbol{\Phi}^{-n}\\ \vdots\\ \mathbf{A}\boldsymbol{\Phi}^{-1}\\ \mathbf{A}\\ \mathbf{A}\boldsymbol{\Phi}\\ \vdots\\ \mathbf{A}\boldsymbol{\Phi}^{n}\end{bmatrix}\in\mathcal{C}^{mM,q}$$

and

$$\mathbf{F}_s=\left[\boldsymbol{\Phi}^n\mathbf{s}\left(\frac{n}{P}\right)\cdots\boldsymbol{\Phi}^{N-n-1}\mathbf{s}\left(\frac{N-n-1}{P}\right)\right]\in\mathcal{C}^{q,N-m+1}$$

is a matrix collecting $N-m+1$ samples of the $q$ sources.

### 2.1.2. Spatial smoothing

In the spatial domain, we employ spatial smoothing technique to separate the coherent signals. In spatial smoothing, an array of $M$ sensors is subdivided into $L$ subarrays. The number of elements in a subarray depends on the way the division is made. For instance, assume that $L$ is odd, namely, $L=2k+1$ $(k=1,2,\ldots)$. The number of elements per subarray is $M_L=M-L+1$. For $l=1,2,\ldots,L$, define the selection matrix $\mathbf{J}_l$ as follows: $\mathbf{J}_l\triangleq\mathbf{I}_m\otimes\mathbf{k}_l$, where $\mathbf{k}_l=[\mathbf{0}_{M_L\times(l-1)}\ \mathbf{I}_{M_L}\ \mathbf{0}_{M_L\times(M-M_L-l+1)}]$ and the operator $\otimes$ denotes the Kronecker matrix product. The selection matrix $\mathbf{J}_l$ selects the part of the $mM\times(N-m+1)$ temporally smoothed data matrix $\mathbf{X}_m$ that correspond to

the $l$ th subarray. Then, an $(m,L)$ factor spatio-temporally smoothed data matrix $\mathbf{X}_{m,L}$ is constructed as [19]

$$\mathbf{X}_{m,L}\triangleq[\mathbf{J}_1\mathbf{X}_m\cdots\mathbf{J}_L\mathbf{X}_m]\in\mathcal{C}^{mM_L,L(N-m+1)}$$

Using the structure of $\mathbf{X}_m$ from (3), this can be factored as

$$\mathbf{X}_{m,L}=[\mathbf{J}_1\mathbf{A}_m\ \cdots\ \mathbf{J}_L\mathbf{A}_m]\begin{bmatrix}\mathbf{F}_s & & \\ & \ddots & \\ & & \mathbf{F}_s\end{bmatrix}+\mathbf{W}_{m,L}$$

where $\mathbf{W}_{m,L}$ is a noise term that has also been shuffled in a similar way as $\mathbf{X}_{m,L}$.

Let

$$\mathbf{A}_{k,m}\triangleq\mathbf{J}_k\mathbf{A}_m=\begin{bmatrix}\mathbf{A}_k\boldsymbol{\Phi}^{-n}\\ \vdots\\ \mathbf{A}_k\boldsymbol{\Phi}^{-1}\\ \mathbf{A}_k\\ \mathbf{A}_k\boldsymbol{\Phi}\\ \vdots\\ \mathbf{A}_k\boldsymbol{\Phi}^{n}\end{bmatrix}\quad(k=1,\ldots,L)$$

where $\mathbf{A}_k=[\mathbf{a}_{M_L}(\mu_1),\ldots,\mathbf{a}_{M_L}(\mu_q)]$ with $\mathbf{a}_{M_L}(\mu)=[e^{-j((M_L-1)/2)\mu},\ldots,\ e^{-j\mu},1,e^{j\mu},\ldots,e^{j((M_L-1)/2)\mu}]^T$. Then, from the shift invariance structure of $\mathbf{A}_m$, it follows that for $i=1,\ldots,k,\ldots,2k+1$

$$\mathbf{J}_i\mathbf{A}_m=\mathbf{A}_{k,m}\boldsymbol{\Theta}^{i-k}$$

where $\boldsymbol{\Theta}=\mathrm{diag}\{[\vartheta_1,\ldots,\vartheta_q]\}$ with $\vartheta_i=\exp\{-j(2\pi f_i d/c)\sin\theta_i\}$ for $i=1,\ldots,q$. Similarly, we refer to matrix $\boldsymbol{\Theta}$ as space factor matrix and its diagonal element as space factor. Thus, $\mathbf{X}_{m,L}$ can be written in a compact form as

$$\mathbf{X}_{m,L}=\mathbf{A}_{k,m}[\boldsymbol{\Theta}^{1-k}\mathbf{F}_s\ \cdots\ \boldsymbol{\Theta}^{k-1}\mathbf{F}_s]+\mathbf{W}_{m,L}\triangleq\mathbf{A}_{k,m}\mathbf{F}_L+\mathbf{W}_{m,L}\tag{4}$$

where $\mathbf{F}_L=[\boldsymbol{\Theta}^{1-k}\mathbf{F}_s\ \cdots\ \boldsymbol{\Theta}^{k-1}\mathbf{F}_s]$.

Define $\mathbf{a}_{mM_L}(\mu,\nu)\in\mathcal{C}^{mM_L,1}$ as

$$\mathbf{a}_{mM_L}(\mu,\nu)\triangleq\begin{bmatrix}\mathbf{a}_{M_L}(\mu)e^{-jn\nu}\\ \vdots\\ \mathbf{a}_{M_L}(\mu)e^{-j\nu}\\ \mathbf{a}_{M_L}(\mu)\\ \mathbf{a}_{M_L}(\mu)e^{j\nu}\\ \vdots\\ \mathbf{a}_{M_L}(\mu)e^{jn\nu}\end{bmatrix}\tag{5}$$

where $\nu=2\pi f/P$, $P$ is the sample rate.

Using the above definition, $\mathbf{A}_{k,m}$ can be expressed as

$$\mathbf{A}_{k,m}=[\mathbf{a}_{mM_L}(\mu_1,\nu_1),\ldots,\mathbf{a}_{mM_L}(\mu_q,\nu_q)]$$

### 2.2. Review of C-JAFE algorithm

We here present a brief development of C-JAFE algorithm [19]. We begin the development by the EVD of matrix $\mathbf{R}=E\{\mathbf{X}_{m,L,fb}\mathbf{X}_{m,L,fb}^H\}$, where $\mathbf{X}_{m,L,fb}=[\mathbf{X}_{m,L}\mathrm{conj}(\mathbf{II}\mathbf{X}_{m,L})]$, $\mathbf{II}$ is an exchange matrix that reverses the ordering of the rows of $\mathbf{X}_{m,L}$. $\mathbf{X}_{m,L}$ is defined by (4). We compute the EVD of $\mathbf{R}$, i.e., $\mathbf{R}=\mathbf{U}_s\boldsymbol{\Lambda}_s\mathbf{U}_s^H+\mathbf{U}_n\boldsymbol{\Lambda}_n\mathbf{U}_n^H$, where $\mathbf{U}_s$ has $q$ columns, spanning the column space of $\mathbf{R}$. Thus, for some nonsingular $q\times q$ matrix $\mathbf{T}$ such that $\mathbf{U}_s=\mathbf{A}_m\mathbf{T}^{-1}$.

We begin the estimation of the parameters by defining two types of selection matrices: a pair to select the submatrices for estimating the time factor matrix $\boldsymbol{\Phi}$ and a pair for estimating space factor matrix $\boldsymbol{\Theta}$

$$\begin{cases}\mathbf{J}_x(\phi)=[\mathbf{I}_m\ \mathbf{0}]\otimes\mathbf{I}_{M_L}\\ \mathbf{J}_y(\phi)=[\mathbf{0}\ \mathbf{I}_m]\otimes\mathbf{I}_{M_L}\end{cases}\begin{cases}\mathbf{J}_x(\theta)=\mathbf{I}_{M_L}\otimes[\mathbf{I}_m\ \mathbf{0}]\\ \mathbf{J}_y(\theta)=\mathbf{I}_{M_L}\otimes[\mathbf{0}\ \mathbf{I}_m]\end{cases}$$

Let

$$\begin{cases}\mathbf{U}_{x,\phi}=\mathbf{J}_x(\phi)\mathbf{U}_s\\ \mathbf{U}_{y,\phi}=\mathbf{J}_y(\phi)\mathbf{U}_s\end{cases}\begin{cases}\mathbf{U}_{x,\theta}=\mathbf{J}_x(\theta)\mathbf{U}_s\\ \mathbf{U}_{y,\theta}=\mathbf{J}_y(\theta)\mathbf{U}_s\end{cases}$$

These data matrices have the following structures:

$$\begin{cases}\mathbf{U}_{x,\phi}=\mathbf{A}_1\mathbf{T}\\ \mathbf{U}_{y,\phi}=\mathbf{A}_1\boldsymbol{\Phi}\mathbf{T}\end{cases}\begin{cases}\mathbf{U}_{x,\theta}=\mathbf{A}_2\mathbf{T}\\ \mathbf{U}_{y,\theta}=\mathbf{A}_2\boldsymbol{\Theta}\mathbf{T}\end{cases}$$

From the above discussions, we have the following equations:

$$\begin{cases}\mathbf{E}_\phi\triangleq\mathbf{U}_{x,\phi}^{\dagger}\mathbf{U}_{y,\phi}=\mathbf{T}\boldsymbol{\Phi}\mathbf{T}^{-1}\\ \mathbf{E}_\theta\triangleq\mathbf{U}_{x,\theta}^{\dagger}\mathbf{U}_{y,\theta}=\mathbf{T}\boldsymbol{\Theta}\mathbf{T}^{-1}\end{cases}$$

It is seen that the data matrices $\mathbf{E}_\phi$ and $\mathbf{E}_\theta$ are jointly diagonalizable by the same matrix $\mathbf{T}$. There are several algorithms to compute this joint diagonalization, e.g., by means of QZ iteration [23,24] or Jacobi iteration [25]. After $\mathbf{T}$ has been found, we also have estimates of $(\theta_i,\phi_i)$ for each of the $q$ sources. This provides with angle and frequency estimates: $\hat{f}_i=\arg(\phi_i)P/2\pi$, $\hat{\vartheta}_i=\arcsin(-\arg(\theta_i)/2\pi\hat{f}_i\times c\times d)$.

## 3. The proposed Unitary-JAFE algorithm

In this section, we firstly discuss a lower computational complexity but higher performance algorithm to solve the joint angle–frequency estimation. Secondly, the Frame–Newton method is developed for solving the EVD problem of the complex unsymmetric matrix. Finally, the computational complexity of the proposed algorithm is addressed.

### 3.1. Unitary-JAFE algorithm

We begin by developing an invariance relationship satisfied by the real-valued manifold that involves only real-valued quantities. Firstly, we define the unitary matrices $\mathbf{Q}_{2n}$ and $\mathbf{Q}_{2n+1}$ as follows:

$$\mathbf{Q}_{2n}=\frac{1}{\sqrt{2}}\begin{bmatrix}\mathbf{I}_n & j\mathbf{I}_n\\ \mathbf{II}_n & -j\mathbf{II}_n\end{bmatrix}$$

$$\mathbf{Q}_{2n+1}=\frac{1}{\sqrt{2}}\begin{bmatrix}\mathbf{I}_n & 0 & j\mathbf{I}_n\\ \mathbf{0}^T & \sqrt{2} & \mathbf{0}^T\\ \mathbf{II}_n & 0 & -j\mathbf{II}_n\end{bmatrix}\tag{6}$$

where $\mathbf{I}_n$ is the $n\times n$ identity matrix. $\mathbf{II}_n$ is the $n\times n$ exchange matrix with ones on its antidiagonal and zeros

elsewhere, namely,

$$\mathbf{\Pi}_n = \begin{bmatrix} & & 1 \\ & 1 & \\ & \cdot & \\ 1 & & \end{bmatrix}$$

Premultiplying $\mathbf{a}_{mM_L}(\mu,\upsilon)$ (which is defined in (5)) by $\mathbf{Q}_{mM_L}^H$ creates the $mM_L \times 1$ real-valued manifold $\mathbf{d}_{mM_L}(\mu,\upsilon)$ as follows:

$$\begin{aligned}\mathbf{d}_{mM_L}(\mu,\upsilon) &= \mathbf{Q}_{mM_L}^H \mathbf{a}_{mM_L}(\mu,\upsilon) \\ &= \sqrt{2}\times[\cos(l\mu+n\upsilon),\ldots,\cos(n\upsilon), \\ &\quad \cos((l-1)\mu-n\upsilon),\ldots,\cos(l\mu-n\upsilon), \\ &\quad \ldots,\cos(\mu+\upsilon),\cos(\upsilon),\ldots,\cos\mu, \\ &\quad 1/\sqrt{2},-\sin(l\mu+n\upsilon),\ldots,-\sin(n\upsilon), \\ &\quad -\sin((l-1)\mu-n\upsilon),\ldots, \\ &\quad -\sin(\mu+\upsilon),-\sin(\upsilon)\cdots,-\sin\mu]^T \end{aligned} \tag{7}$$

where $l=(M_L-1)/2$.

Let the four selection matrices $\mathbf{KJ}_1,\ldots,\mathbf{KJ}_4$ such that

$$\begin{cases}\mathbf{KJ}_1 = [\mathbf{I}_{m-1}\ \ \mathbf{0}_1]\otimes\mathbf{I}_{M_L} \\ \mathbf{KJ}_2 = [\mathbf{0}_1\ \ \mathbf{I}_{m-1}]\otimes\mathbf{I}_{M_L}\end{cases} \tag{8}$$

$$\begin{cases}\mathbf{KJ}_3 = \mathbf{I}_m\otimes[\mathbf{I}_{M_L-1}\ \ \mathbf{0}_1] \\ \mathbf{KJ}_4 = \mathbf{I}_m\otimes[\mathbf{0}_1\ \ \mathbf{I}_{M_L-1}]\end{cases} \tag{9}$$

form shift invariant pairs. Note that $\mathbf{KJ}_1,\ldots,\mathbf{KJ}_4$ have the following relationship:

$$\begin{cases}\mathbf{KJ}_2 = \mathbf{\Pi}_{(m-1)M_L}\mathbf{KJ}_1\mathbf{\Pi}_{mM_L} \\ \mathbf{KJ}_4 = \mathbf{\Pi}_{m(M_L-1)}\mathbf{KJ}_3\mathbf{\Pi}_{mM_L}\end{cases} \tag{10}$$

From (7) to (10), it can be easily seen that

$$\begin{cases}e^{j\upsilon}\mathbf{KJ}_1\mathbf{a}_{mM_L}(\mu,\upsilon) = \mathbf{KJ}_2\mathbf{a}_{mM_L}(\mu,\upsilon) \\ e^{j\mu}\mathbf{KJ}_3\mathbf{a}_{mM_L}(\mu,\upsilon) = \mathbf{KJ}_4\mathbf{a}_{mM_L}(\mu,\upsilon)\end{cases}$$

Since $\mathbf{Q}_{mM_L}$ is unitary, it follows that

$$e^{j\upsilon}\mathbf{KJ}_1\mathbf{Q}_{mM_L}\mathbf{Q}_{mM_L}^H\mathbf{a}_{mM_L}(\mu,\upsilon) = \mathbf{KJ}_2\mathbf{Q}_{mM_L}\mathbf{Q}_{mM_L}^H\mathbf{a}_{mM_L}(\mu,\upsilon)$$

which, invoking the definition of $\mathbf{d}_{mM_L}(\mu,\upsilon)$ in (7), implies $e^{j\upsilon}\mathbf{KJ}_1\mathbf{Q}_{mM_L}\mathbf{d}_{mM_L}(\mu,\upsilon) = \mathbf{KJ}_2\mathbf{Q}_{mM_L}\mathbf{d}_{mM_L}(\mu,\upsilon)$. Premultiplying both sides by $\mathbf{Q}_{(m-1)M_L}^H$ yields the following invariance relationship:

$$e^{\,j\upsilon}\mathbf{Q}_{(m-1)M_L}^H\mathbf{KJ}_1\mathbf{Q}_{mM_L}\mathbf{d}_{mM_L}(\mu,\upsilon) = \mathbf{Q}_{(m-1)M_L}^H\mathbf{KJ}_2\mathbf{Q}_{mM_L}\mathbf{d}_{mM_L}(\mu,\upsilon) \tag{11}$$

Note that $\mathbf{KJ}_1$ and $\mathbf{KJ}_2$ satisfy $\mathbf{KJ}_2 = \mathbf{\Pi}_{(m-1)M_L}\mathbf{KJ}_1\mathbf{\Pi}_{mM_L}$. As a consequence,

$$\begin{aligned}\mathbf{Q}_{(m-1)M_L}^H\mathbf{KJ}_2\mathbf{Q}_{mM_L} &= \mathbf{Q}_{(m-1)M_L}^H\mathbf{\Pi}_{(m-1)M_L} \\ &\quad\times\mathbf{\Pi}_{(m-1)M_L}\mathbf{KJ}_2\mathbf{\Pi}_{mM_L}\mathbf{\Pi}_{mM_L}\mathbf{Q}_{mM_L} \\ &= \mathbf{Q}_{(m-1)M_L}^T\mathbf{KJ}_1\mathbf{Q}_{mM_L}^* \\ &= (\mathbf{Q}_{(m-1)M_L}^H\mathbf{KJ}_1\mathbf{Q}_{mM_L})^*\end{aligned}$$

Let $\mathbf{K}_1$ and $\mathbf{K}_2$ be the real and imaginary parts of $\mathbf{Q}_{(m-1)M_L}^H\mathbf{KJ}_2\mathbf{Q}_{mM_L}$, respectively, as follows:

$$\begin{cases}\mathbf{K}_1 = \mathrm{Re}\{\mathbf{Q}_{(m-1)M_L}^H\mathbf{KJ}_2\mathbf{Q}_{mM_L}\} \\ \mathbf{K}_2 = \mathrm{Im}\{\mathbf{Q}_{(m-1)M_L}^H\mathbf{KJ}_2\mathbf{Q}_{mM_L}\}\end{cases}$$

With these definitions, (11) can be expressed as $e^{j\upsilon/2}(\mathbf{K}_1 - j\mathbf{K}_2)\mathbf{d}_{mM_L}(\mu,\upsilon) = e^{-j\upsilon/2}(\mathbf{K}_1 + j\mathbf{K}_2)\mathbf{d}_{mM_L}(\mu,\upsilon)$. Rearranging, we have $(e^{j\upsilon/2} - e^{-j\upsilon/2})\mathbf{K}_1\mathbf{d}_{mM_L}(\mu,\upsilon) = j(e^{j\upsilon/2} + e^{-j\upsilon/2})\mathbf{K}_2\mathbf{d}_{mM_L}(\mu,\upsilon)$. Invoking the definition of the tangent function yields the following invariance relationship satisfied by $\mathbf{d}_{mM_L}(\mu,\upsilon)$ involving only real-valued quantities:

$$\tan\left(\frac{\upsilon}{2}\right)\mathbf{K}_1\mathbf{d}_{mM_L}(\mu,\upsilon) = \mathbf{K}_2\mathbf{d}_{mM_L}(\mu,\upsilon) \tag{12}$$

For $q<((m-1)M_L)$ sources, we define the $mM_L\times q$ real-valued DOA matrix as $\mathbf{D} = [\mathbf{d}_{mM_L}(\mu_1,\upsilon_1),\ldots,\mathbf{d}_{mM_L}(\mu_q,\upsilon_q)]$. The real-valued manifold relation in (12) translates into the real-valued DOA matrix relation

$$\mathbf{K}_1\mathbf{D}\mathbf{\Omega}_\upsilon = \mathbf{K}_2\mathbf{D} \tag{13}$$

where $\mathbf{\Omega}_\upsilon = \mathrm{diag}\{[\tan(\upsilon_1/2),\ldots,\tan(\upsilon_q/2)]\}$.

Similarly, we have the following relation:

$$\mathbf{K}_3\mathbf{D}\mathbf{\Omega}_\mu = \mathbf{K}_4\mathbf{D} \tag{14}$$

where $\mathbf{\Omega}_\mu = \mathrm{diag}\{[\tan(\mu_1/2),\ldots,\tan(\mu_q/2)]\}$. $\mathbf{K}_3,\mathbf{K}_4$ is the real and imaginary parts of $\mathbf{Q}_{(m-1)M_L}^H\mathbf{KJ}_4\mathbf{Q}_{mM_L}$, respectively, as follows:

$$\begin{cases}\mathbf{K}_3 = \mathrm{Re}\{\mathbf{Q}_{(m-1)M_L}^H\mathbf{KJ}_4\mathbf{Q}_{mM_L}\} \\ \mathbf{K}_4 = \mathrm{Im}\{\mathbf{Q}_{(m-1)M_L}^H\mathbf{KJ}_4\mathbf{Q}_{mM_L}\}\end{cases}$$

Finally, performing forward–backward averaging on $\mathbf{X}_{m,L}$, we get the $mM_L\times 2L(N-m+1)$ data matrix

$$\mathbf{X}_{m,L,fb} = [\mathbf{X}_{m,L}\ \ \mathrm{conj}(\mathbf{\Pi}\mathbf{X}_{m,L})] \tag{15}$$

where $\mathbf{\Pi}$ is an exchange matrix that reverses the ordering of the rows of $\mathbf{X}_{m,L}$.

Assume that the eigenvalue decomposition of the covariance matrix $\mathbf{R} = \mathbf{Y}\mathbf{Y}^H$ ($\mathbf{Y} = [\mathrm{Re}\{\mathbf{X}\},\mathrm{Im}\{\mathbf{X}\}]$, $\mathbf{X} = \mathbf{Q}_{mM_L}^H\mathbf{X}_{m,L,fb}$) has the following expression:

$$\mathbf{R} = \sum_{k=1}^{mM_L}\lambda_k\mathbf{u}_k\mathbf{u}_k^H = \mathbf{U}_s\mathbf{\Lambda}_s\mathbf{U}_s^H + \mathbf{U}_n\mathbf{\Lambda}_n\mathbf{U}_n^H$$

where $\lambda_1\geq\cdots\geq\lambda_q>\lambda_{q+1}=\cdots=\lambda_{mM_L}$, $\mathbf{U}_s = [\mathbf{u}_1,\ldots,\mathbf{u}_q]$, $\mathbf{U}_n = [\mathbf{u}_{q+1},\ldots,\mathbf{u}_{mM_L}]$.

Since $\mathrm{span}\{\mathbf{U}_s\} = \mathrm{span}\{\mathbf{D}\}$, there must exist a unique nonsingular real-valued matrix $\mathbf{T}$ such that $\mathbf{U}_s = \mathbf{D}\mathbf{T}$. Substituting $\mathbf{D} = \mathbf{U}_s\mathbf{T}^{-1}$ into (13) and (14) yields the signal eigenvector relations

$$\begin{cases}\mathbf{K}_1\mathbf{U}_s\mathbf{\Psi}_\upsilon = \mathbf{K}_2\mathbf{U}_s \\ \mathbf{K}_3\mathbf{U}_s\mathbf{\Psi}_\mu = \mathbf{K}_4\mathbf{U}_s\end{cases} \tag{16}$$

where $\mathbf{\Psi}_\upsilon = \mathbf{T}^{-1}\mathbf{\Omega}_\upsilon\mathbf{T}$ and $\mathbf{\Psi}_\mu = \mathbf{T}^{-1}\mathbf{\Omega}_\mu\mathbf{T}$.

Automatic pairing of $\mu$ and $\upsilon$ parameter estimates is facilitated by the fact that all of the quantities in (16) are real valued. Thus, $\mathbf{\Psi} = \mathbf{\Psi}_\upsilon + j\mathbf{\Psi}_\mu$ may be decomposed as

$$\mathbf{\Psi} = \mathbf{\Psi}_\upsilon + j\mathbf{\Psi}_\mu = \mathbf{T}^{-1}(\mathbf{\Omega}_\upsilon + j\mathbf{\Omega}_\mu)\mathbf{T} \tag{17}$$

By Eq. (16), it is clear that the matrix $\mathbf{\Psi}$ includes the information of DOAs and frequencies of incident signal sources. Therefore, we refer to the matrix $\mathbf{\Psi}$ as the space–time factor matrix and its diagonal element as space–time factor.

**Summary of Unitary-JAFE**:

(1) Collect the data and estimate $\mathbf{R}=E\{\mathbf{YY}^H\}(\mathbf{Y}=[\mathrm{Re}\{\mathbf{X}\},\mathrm{Im}\{\mathbf{X}\}],\mathbf{X}=\mathbf{Q}_{mM_L}^H\mathbf{X}_{m,L,fb})$ denoting the estimate $\hat{\mathbf{R}}$.
(2) Compute the eigendecomposition of $\hat{\mathbf{R}}=\sum_{k=1}^{mM_L}\hat{\lambda}_k\hat{\mathbf{u}}_k\hat{\mathbf{u}}_k^H$, where $\hat{\lambda}_1,\geq,\ldots,\geq\hat{\lambda}_{mM_L}$.
(3) Estimate the number of sources $\hat{q}$ by the maximum eigenvalue of $\hat{\mathbf{R}}$ according to AIC [26], if $q$ is unknown.
(4) Obtain the signal subspace estimate $\hat{\mathbf{U}}_s$ via $\hat{q}$ "largest" eigenvectors of $\hat{\mathbf{R}}$.
(5) Calculate $\hat{\boldsymbol{\Psi}}_v$ as the solution to the matrix equation $\mathbf{K}_1\hat{\mathbf{U}}_s\boldsymbol{\Psi}_v=\mathbf{K}_2\hat{\mathbf{U}}_s$.
(6) Calculate $\hat{\boldsymbol{\Psi}}_\mu$ as the solution to the matrix equation $\mathbf{K}_3\hat{\mathbf{U}}_s\boldsymbol{\Psi}_\mu=\mathbf{K}_4\hat{\mathbf{U}}_s$.
(7) Compute $\hat{\gamma}_k$ $(k=1,\ldots,q)$ as the eigenvalues of the space–time factor matrix $\hat{\boldsymbol{\Psi}}=\hat{\boldsymbol{\Psi}}_v+j\hat{\boldsymbol{\Psi}}_\mu$.
(8) Compute spatial frequency estimates

$$\begin{cases}\hat{v}_k=2\arctan(\mathrm{Re}\{\hat{\gamma}_k\})\\ \hat{\mu}_k=2\arctan(\mathrm{Im}\{\hat{\gamma}_k\})\end{cases}$$

(9) Estimate the frequency and DOA

$$\begin{cases}\hat{f}_k=\dfrac{\hat{v}_k}{2\pi}\times P\\ \hat{\theta}_k=\arcsin\left(\hat{\mu}_k\times\dfrac{c}{2\pi d\hat{f}_k}\right)\end{cases}$$

### 3.2. Frame–Newton method

As discussed above, in the final stage of the Unitary-JAFE algorithm, the matrix required to eigendecomposition is a complex unsymmetric matrix. In this section, we consider the eigendecomposition problem for a complex unsymmetric matrix.

#### 3.2.1. Frame method

First of all, let us review the definitions about the minimal polynomial and the characteristic polynomial.

**Definition 3.1** (*Hefferon [27]*). The minimal polynomial $m(\lambda)$ of a transformation $t$ or a square matrix $\mathbf{A}$ is the polynomial of least degree and with leading coefficient 1 such that $m(t)$ is the zero map or $m(\mathbf{A})$ is the zero matrix.

**Definition 3.2** (*Hefferon [27]*). The characteristic polynomial $f(\lambda)$ of a square matrix $\mathbf{A}$ is the determinant of the matrix $\mathbf{A}-\lambda\mathbf{I}$, namely, $f(\lambda)=|\mathbf{A}-\lambda\mathbf{I}|$, where $\lambda$ is a variable. The characteristic equation is $|\mathbf{A}-\lambda\mathbf{I}|=\mathbf{0}$.

**Theorem 3.1.** *Assume that there are q narrow-band sources, with the complex baseband representations $s_i(t)$ $(i=1,\ldots,q)$, such that the ith source has a carrier frequency of $f_i$ and arrives a ULA from direction $\theta_i$. If the q sources are not equal in both of the carrier frequency f and the angle of incidence $\theta$, then the minimal polynomial $m(\lambda)$ and the characteristic polynomial $f(\lambda)$ of the matrix $\boldsymbol{\Psi}\in\mathcal{C}^{q\times q}$ has the following relationship $m(\lambda)=f(\lambda)$, where the matrix $\boldsymbol{\Psi}=\boldsymbol{\Psi}_v+j\boldsymbol{\Psi}_u$ is a complex unsymmetric matrix in the final stage of the Unitary-JAFE.*

**Proof.** See Appendix A.

Let $\mathbf{A}$ be an $n\times n$ complex matrix, suppose that $\lambda_1,\ldots,\lambda_n$ are the eigenvalues of matrix $\mathbf{A}$ and $f(\lambda)=\lambda^n+a_1\lambda^{n-1}+\cdots+a_{n-1}\lambda+a_n$ is the characteristic polynomial of matrix $\mathbf{A}$. Let $s_k=\lambda_1^k+\lambda_2^k+\cdots+\lambda_n^k$. Then, we have the following Newton's identities [28]:

$$\begin{cases}-a_1=s_1\\ -ka_k=s_k+a_1s_{k-1}+\cdots+a_{k-1}s_1\quad(k=2,3,\ldots,n)\end{cases}\tag{18}$$

According to the Eq. (18), we have the following Frame algorithm [28]:

$$\left.\begin{array}{lll}\mathbf{A}_1=\mathbf{A}, & p_1=\mathrm{trace}(\mathbf{A}_1), & \mathbf{B}_1=\mathbf{A}_1-p_1\mathbf{I}\\ \mathbf{A}_2=\mathbf{AB}_1, & p_2=\dfrac{1}{2}\mathrm{trace}(\mathbf{A}_2), & \mathbf{B}_2=\mathbf{A}_2-p_2\mathbf{I}\\ \vdots & \vdots & \vdots\\ \mathbf{A}_n=\mathbf{AB}_{n-1}, & p_n=\dfrac{1}{n}\mathrm{trace}(\mathbf{A}_n), & \mathbf{B}_n=\mathbf{A}_n-p_n\mathbf{I}\end{array}\right\}\tag{19}$$

**Lemma 3.1** (*Zhang and Xu [28]*). *From the Frame algorithm* (19), *each of the following is true.*

(1) $a_k=-p_k$, $(k=1,2,\ldots,n)$, *where $a_k$ is the coefficient of the characteristic polynomial $f(\lambda)$. $p_k$ is defined by the Frame algorithm* (19);
(2) $\mathbf{B}_n=\mathbf{0}$;
(3) *If* $\mathbf{A}$ *is a nonsingular matrix, then* $\mathbf{A}^{-1}=(1/p_n)\mathbf{B}_{n-1}$.

**Lemma 3.2** (*Zhang and Xu [28]*). *Let*

$$\mathbf{Q}_k=\lambda_k^{n-1}\mathbf{I}+\lambda_k^{n-2}\mathbf{B}_1+\cdots+\lambda_k\mathbf{B}_{n-2}+\mathbf{B}_{n-1}\tag{20}$$

*If $\mathbf{Q}_k$ is not a zero matrix, then the nonzero column vector of matrix $\mathbf{Q}_k$ is the eigenvector of* $\mathbf{A}$, *and the corresponding eigenvalue is $\lambda_k$.*

**Lemma 3.3** (*Zhang and Xu [28]*). *Let $m(\lambda)$ and $f(\lambda)$ be the minimal polynomial and characteristic polynomial of* $\mathbf{A}$, *respectively. If $m(\lambda)=f(\lambda)$, then $\mathbf{Q}_k=\lambda_k^{n-1}\mathbf{I}+\lambda_k^{n-2}\mathbf{B}_1+\cdots+\lambda_k\mathbf{B}_{n-2}+\mathbf{B}_{n-1}\neq\mathbf{0}$.*

From Theorem 3.1, Lemma 3.1–3.3 and the Frame algorithm, we have the following Theorem 3.2.

**Theorem 3.2.** *Assume that there are q narrow-band sources, with the complex baseband representations $s_i(t)$ $(i=1,\ldots,q)$, such that the ith source has a carrier frequency of $f_i$ and arrives a ULA from direction $\theta_i$. If the q sources are not equal in both of the carrier frequency f and the angle of incidence $\theta$, then each of the following is true:*

(1) *$a_k=-p_k$, where $a_k$ is the coefficient of the characteristic polynomial $f(\lambda)$ of $\boldsymbol{\Psi}$ and $p_k$ is defined by the Frame algorithm* (19).
(2) *The nonzero column vector of $\mathbf{Q}_k$ is the eigenvector of $\boldsymbol{\Psi}$, and the corresponding eigenvalue is $\lambda_k$. Where the matrix $\boldsymbol{\Psi}=\boldsymbol{\Psi}_v+j\boldsymbol{\Psi}_u$ is a complex unsymmetric matrix in the final stage of the Unitary-JAFE.*

**Proof.** The fact that (1) $a_k = -p_k$ is established simply by Lemma 3.1.

It is clear that $m(\lambda) = f(\lambda)$ by Theorem 3.1, where $m(\lambda)$ and $f(\lambda)$ are the minimal polynomial and characteristic polynomial of $\mathbf{\Psi}$, respectively. Then, Lemma 3.3 guarantees that $\mathbf{Q}_k \neq \mathbf{0}$. Thus, making use of Lemma 3.2, we can conclude that (2) the nonzero column vector of $\mathbf{Q}_k$ is the eigenvector of $\mathbf{\Psi}$. □

*3.2.2. Frame–Newton algorithm*

As described in Section 3.2.1, the eigendecomposition of a complex matrix $\mathbf{A}$ involves three main steps, namely

(1) Obtain the characteristic polynomial $f(\lambda) = \lambda^n + a_1 \lambda^{n-1} + \cdots + a_{n-1}\lambda + a_n$ of $\mathbf{A} \in \mathcal{C}^{n\times n}$.
(2) Calculate the roots of the algebraic equation $f(\lambda) = 0$, namely, the eigenvalues of $\mathbf{A}$.
(3) Compute the eigenvectors of $\mathbf{A}$.

Theorem 3.2 shows that the coefficients $a_1, \ldots, a_n$ can be obtained by computing $p_1, \ldots, p_n$, which are defined in (19). Notice that $f(\lambda) = 0$ is a algebraic equation with complex coefficients. Making use of the Newton-downhill method [29], we can solve the algebraic equation to obtain the eigenvalue $\lambda_k$ $(k = 1, \ldots, n)$ of matrix $\mathbf{A}$. Finally, we may use the nonzero column vector of matrix $\mathbf{Q}_k$ to obtain the eigenvectors of $\mathbf{A}$.

For computing the eigenvalues and eigenvectors of a complex unsymmetric matrix, the Frame–Newton algorithm is summarized as follows.

**Frame–Newton algorithm**.

*Step* 1: By the Frame algorithm, compute the coefficients $a_1, \ldots, a_n$ of the characteristic polynomial $f(\lambda) = \lambda^n + a_1\lambda^{n-1} + \cdots + a_{n-1}\lambda + a_n$ of $\mathbf{A} \in \mathcal{C}^{n\times n}$.

*Step* 2: Making use of the Newton-downhill method, calculate the roots of the algebraic equation $f(\lambda) = 0$, namely, the eigenvalues of $\mathbf{A}$.

*Step* 3: By the nonzero column vector of $\mathbf{Q}_k$ in the Frame algorithm, obtain the eigenvectors of $\mathbf{A}$.

### 3.3. Computational complexity

We briefly investigate the computational complexity of the proposed algorithm. We use $\mathcal{O}(M^3)$ to represent the order of $M^3$ real multiplications. The Unitary-JAFE algorithm consists of mainly three computational steps: an eigendecomposition of a real-valued matrix $\mathbf{R}$ (size $N \times N$, where $N = mM_L$ with $m$ and $M_L$ standing for the number of temporal smoothed data and isotropic sensors, respectively), Moore–Penrose inverses of the two real-valued matrices $\mathbf{U}_1 = \mathbf{K}_1\mathbf{U}_s$ and $\mathbf{U}_3 = \mathbf{K}_3\mathbf{U}_s$ (size $N \times q$, where $q$ is the total number of signal sources present in the ULA), an eigendecomposition of a complex unsymmetric matrix $\mathbf{\Psi}$ (size $q \times q$). Since we require $N > q$, the first EVD is the most expensive and the complexity of this step is $\mathcal{O}(N^3)$. In the second step, the computation of $\mathbf{X}^\dagger = \mathbf{X}^T(\mathbf{X}\mathbf{X}^T)^{-1}$ (where $\mathbf{X} = \mathbf{U}_1$ or $\mathbf{U}_3$) calls for about $2N^2q$ real multiplications (ignoring the inversion). The complexity of EVD of the complex unsymmetric matrix $\mathbf{\Psi}$ is $\mathcal{O}(8q^3)$. Table 1 presents the computational complexity of the previous algorithms and the proposed method, including the aforementioned three main steps. $g_s$ and $g_f$ are the numbers of searches conducted along the DOA axis and the frequency axis, respectively. $L$ is the sample number.

## 4. Simulation results

In this section, we construct several simulations to evaluate the proposed algorithm.

### 4.1. Signal reconstruction

First, we examine the effect of Unitary-JAFE on the resulting signal estimates. Assume that there are three far field uncorrelated equi-powered BPSK signals impinging on a ULA which consists of $M = 7$ sensors. The three BPSK signals arrive from $\theta_1 = -30^\circ$, $\theta_2 = 0^\circ$, $\theta_3 = 30^\circ$, respectively. Their corresponding center frequency are $f_1 = 50\,\text{MHz}$, $f_2 = 40\,\text{MHz}$, $f_3 = 40\,\text{MHz}$, respectively. In the simulations, the temporal and spatial smoothing factors are chosen to be $m = 3$ and $L = 3$, respectively. Fig. 1 shows the resulting output signal-to-noise-and-interference ratio (SNIR) as a function of the signal-to-noise ratio (SNR) and the number of snapshots $N$ using C-JAFE (dashed lines) and Unitary-JAFE (solid lines). The values of $Nu$ correspond to the solid lines, i.e., Unitary-JAFE. The output SNIR achieved by the C-JAFE algorithm for a given valued of $Nc$ (dashed lines) can be found below the corresponding solid lines. For small values of $N$, e.g., $Nu =$ 10 snapshots, Unitary-JAFE achieves a significantly better performance than the C-JAFE algorithm. Notice that C-JAFE with $Nc = 20$ snapshots attains the same performance as Unitary-JAFE with $Nu = 10$ snapshots for SNRs that are greater than 11 dB, while the performance of C-JAFE with $Nc = 40$ is comparable to the performance of Unitary-JAFE with $Nu = 20$ for SNR's that are greater than 7 dB. Thus, Unitary-JAFE algorithm essentially doubles the number of available snapshots $N$ compared to the C-JAFE algorithm.

### 4.2. DOA and frequency estimation

Next, we investigate the effect of Unitary-JAFE on the estimated DOA $\theta_k$ and frequency $f_k$, $k = 1, \ldots, q$. Consider a seven-element ULA with baseline separation of $\Delta = 30\,\text{m}$. Assume that three far field equal power signals $s_1$, $s_2$, $s_3$ are impinging on the antenna array. Their DOAs are $\theta_1 = 50^\circ$, $\theta_2 = 30^\circ$, $\theta_3 = -30^\circ$, respectively. Their corresponding center frequencies are $f_1 = 5\,\text{MHz}$, $f_2 = 4\,\text{MHz}$, $f_3 = 2.5\,\text{MHz}$, respectively. The source signals are narrowband (25 kHz) amplitude-modulated signals. The data are sampled at a rate of 15 MHz. In the simulations, the temporal and spatial smoothing factors are chosen to be $m = 3$ and $L = 3$, respectively.

For an ULA, the form of the true eigenvalues of the space–time factor matrix $\mathbf{\Psi}$ in the final stage of Unitary-JAFE, is shown in the complex plane as depicted in Fig. 2(a). The eigenvalues of the space–time factor matrix $\mathbf{\Psi}$, estimated with Unitary-JAFE algorithm based on Frame–Newton method, are shown in Fig. 2(b). The

results of 100 trial runs with $N = 50$ snapshots and a SNR of 0 dB are shown. Notice that all eigenvalues of the space–time factor matrix $\mathbf{\Psi}$ estimated with Unitary-JAFE are obtained accurately and are very close to the true eigenvalues. The form of the true diagonal elements of the time factor matrix and the time factors $\phi_1,\ \phi_2,\ \phi_3$ estimated with the C-JAFE algorithm, e.g. by means of joint diagonalization based on QZ iteration are as shown in Fig. 3(a) and (b), respectively, for sources $s_1,\ s_2,\ s_3$. The form of the true diagonal elements of the space factor matrix and the space factors $\vartheta_1,\ \vartheta_2,\ \vartheta_3$ estimated with the C-JAFE algorithm, e.g. by means of joint diagonalization based on QZ iteration are given in the complex plane as depicted in Fig. 4(a) and (b), respectively. Figs. 3(a) and 4(a) show that the time factor and space factor of interest ideally lie on the unit circle and are related one-to-one with each source. As shown in Figs. 3(b) and 4(b), the C-JAFE algorithm reliability test has failed many times. Notice that the variance of the DOA and frequency estimates that pass the Unitary-JAFE reliability test is much lower than the variance of the DOA and frequency estimates obtained by the C-JAFE. The advantages of Unitary-JAFE become even more evident if the root-mean-squared-error (RMSE) of the estimated eigenvalues of the space–time factor matrix is plotted as function of the SNR. The RMSE is defined as $\sqrt{E\{\sum_{k=1}^{q}(\hat{\psi}_k-\psi_k)^2\}}$ ($\psi_k$ is the space–time factor) and $\sqrt{E\{\sum_{k=1}^{q}((\hat{\phi}_k-\phi_k)^2+(\hat{\vartheta}_k-\vartheta_k)^2)\}}$ ($\phi_k$ and $\vartheta_k$ stand for the time factor and space factor, respectively), for the Unitary-JAFE algorithm based on the Frame–Newton method and the C-JAFE algorithm based on the joint

**Table 1**
Comparison of the computational complexity of the proposed algorithm with other previous algorithms.

| Algorithms | EVD | Moore–Penrose | Other processing |
|---|---|---|---|
| Unitary-JAFE | $\mathcal{O}(N^3)+\mathcal{O}(8q^3)$ | $\mathcal{O}(2N^2q)$ | Without |
| C-JAFE | $\mathcal{O}(8N^3)$ | $\mathcal{O}(8N^2q)$ | Joint diagonalization $\mathcal{O}(4q^4)$<br>Pairing processing $\mathcal{O}(8q^3)$ |
| FSF-ESPRIT | $\mathcal{O}(8N^3)+\mathcal{O}(8q^3)$ | Without | Temporal filtering $\mathcal{O}(N^2)$<br>Spatial beamforming $\mathcal{O}(L^2)$<br>1-D search $\mathcal{O}(N^2g_s)+\mathcal{O}(L^2g_f)$ |
| FSF-MUSIC | $\mathcal{O}(8N^3)+\mathcal{O}(8q^3)$ | Without | Temporal filtering $\mathcal{O}(N^2)$<br>Spatial beamforming $\mathcal{O}(L^2)$ |

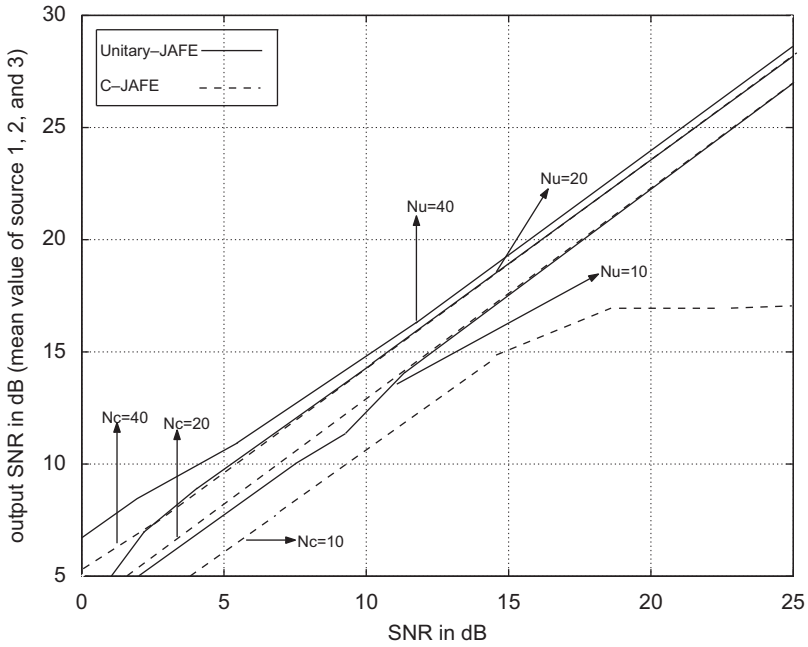


**Fig. 1.** Output SNIR as function of the SNR and the number of snapshots $N$ using C-JAFE (dashed lines) and Unitary-JAFE (solid lines) for $\theta_1 = -30^\circ$, $\theta_2 = 0^\circ$, $\theta_3 = 30^\circ$ and $f_1 = 50$ MHz, $f_2 = f_3 = 40$ MHz ($M = 7$ sensors, 500 trial runs). The values of $Nu$ correspond to the solid lines, i.e., Unitary-JAFE. The output SNIR achieved by the C-JAFE for a given value of $Nc$ (dashed lines) can be found below the corresponding solid lines.

diagonalization, respectively. Fig. 5 shows these curves with SNRs ranging from −15 to 20 dB using 1000 trial runs. The solid line stands for the RMSE curve of the space–time factors estimated with the Unitary-JAFE algorithm based on Frame–Newton method. The dashed line presents the RMSE curve of the space factor and time

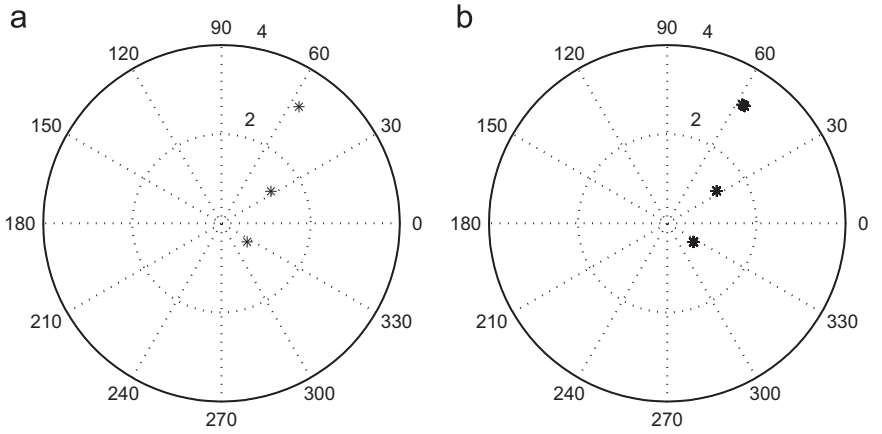


**Fig. 2.** Comparison of (a) the form of the true eigenvalues of the space–time factor matrix $\mathbf{\Psi}$ and (b) the eigenvalues of the space–time factor matrix $\mathbf{\Psi}$ estimated with Unitary-JAFE based on Frame–Newton method, for sources $s_1,\ s_2,\ s_3$ ($M = 7$ sensors, $m = L = 3$, SNR = 0 dB, $N = 50$, 100 trial runs).

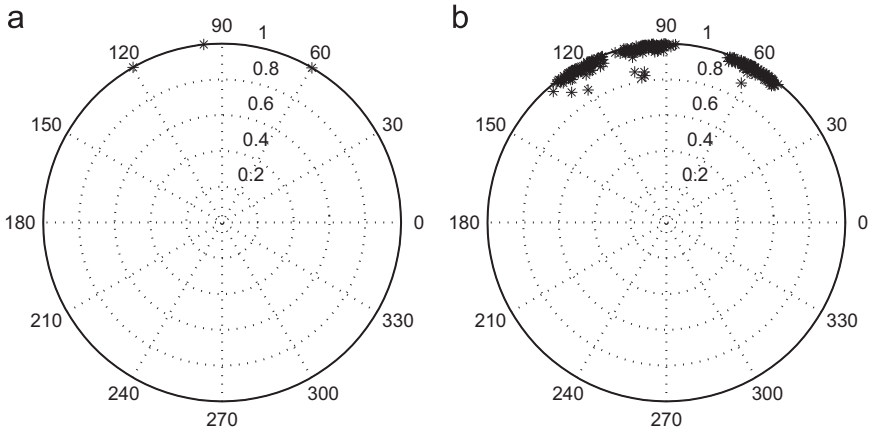


**Fig. 3.** Comparison of (a) the form of the true time factor and (b) the time factor estimated with C-JAFE algorithm, e.g. by means of joint diagonalization based on QZ iteration ($M = 7$ sensors, $m = L = 3$, SNR = 0 dB, $N = 50$, 100 trial runs), for sources $s_1,\ s_2,\ s_3$.

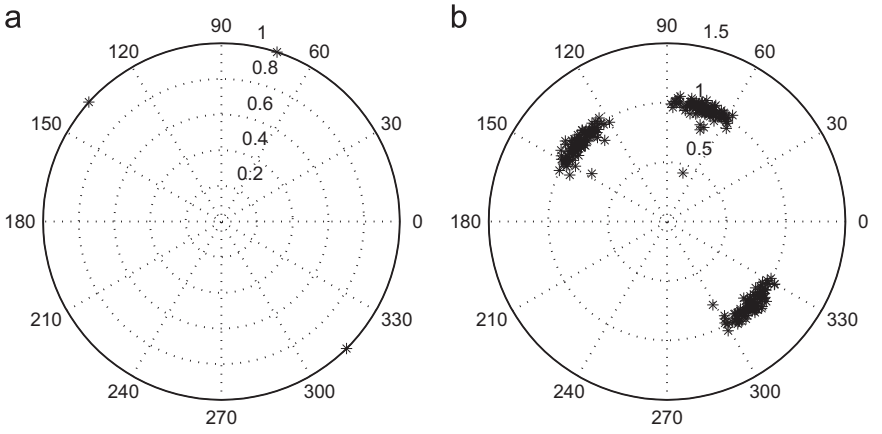


**Fig. 4.** Comparison of (a) the form of the true space factor and (b) the space factor estimated with C-JAFE algorithm, e.g. by means of joint diagonalization based on QZ iteration ($M = 7$ sensors, $m = L = 3$, SNR = 0 dB, $N = 50$, 100 trial runs), for sources $s_1,\ s_2,\ s_3$.

factor estimated with the C-JAFE algorithm based on the joint diagonalization. It can be seen that Unitary-JAFE algorithm based on Frame–Newton method improves the estimation accuracy considerably.

Four algorithms are carried out for comparison, including the C-JAFE algorithm [19], the FSF-ESPRIT algorithm [30], the proposed Unitary-JAFE algorithm, and the FSF-MUSIC algorithm [6]. The Cramer–Rao low bound (CRLB) given in [31,32] is also furnished for reference. For a clear illustration, only the RMSEs of the DOA and frequency estimates of the first signal source $s_1(t)$ are provided, as shown in Figs. 6 and 7. For each specific SNR, 500 Monte Carlo trials are carried out. From Figs. 6 and 7, we can note that FSF-MUSIC algorithm outperforms the C-JAFE, FSF-ESPRIT, and Unitary-JAFE algorithms in DOA and frequency estimates. However, the FSF-MUSIC algorithm requires multiple 1-D peak search in space domain and frequency domain so that

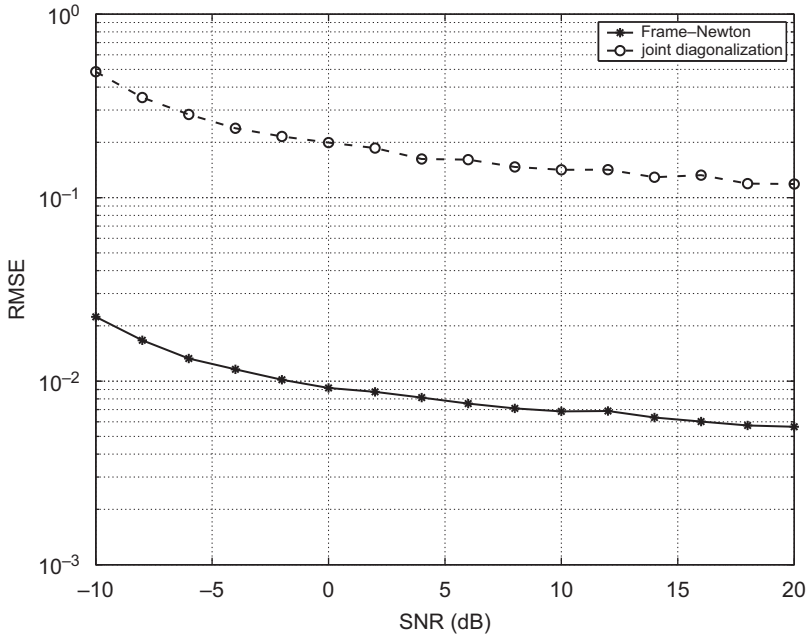


**Fig. 5.** Comparison of the RMSE of the estimated eigenvalues between the Frame–Newton method and the joint diagonalization based on QZ iteration.

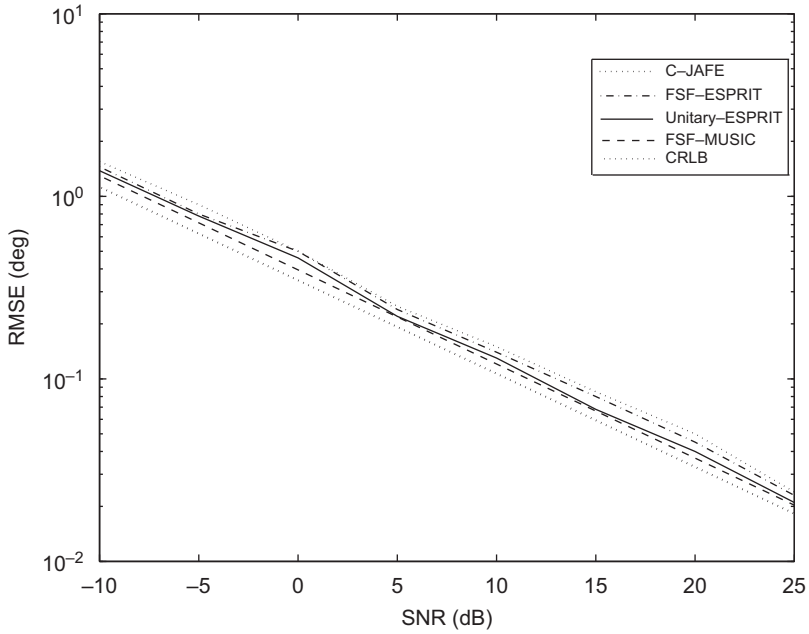


**Fig. 6.** RMSE curves for frequency estimation.

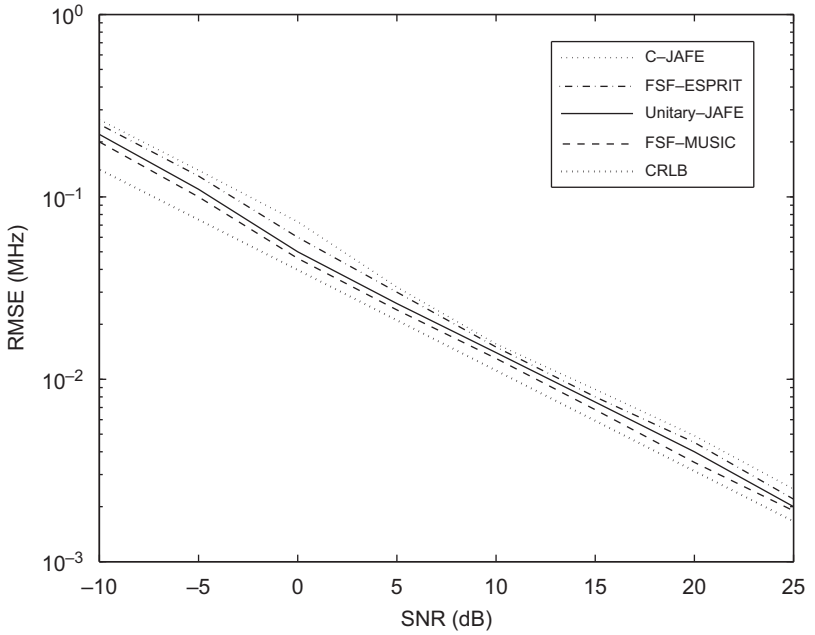


**Fig. 7.** RMSE curves for DOA estimation.

its computation complexity is not very attractive. As shown in these figures, the performance of the proposed algorithm is superior to that of the C-JAFE and FSF-ESPRIT algorithms.

## 5. Conclusions

In this paper, an Unitary-JAFE algorithm based on Frame–Newton method is proposed for joint angle–frequency estimation. In this proposed method, the computational complexity is reduced significantly by the real-valued computation, except for the final eigenvalue decomposition. Unitary-JAFE represents a simple method to constrain the estimated signal parameters to the complex eigenvalues of the space–time factor matrix, yielding more accurate signal subspace estimates and avoiding the complex joint diagonal processing. In the final stage of the proposed algorithm, the real and imaginary parts of the $i$ th eigenvalue of the space–time factor matrix are one-to-one related to the frequency and DOA of the $i$ th source, respectively. That is, the pairing of the estimated frequency and DOA is automatically determined. Compared with the previous works, the presented method has lower computational complexity, but it exhibits superior performance, such as smaller estimation error and better robustness to SNR change, etc.

## Appendix A

### A.1. Proof of Theorem 3.1

Let $\lambda_1,\ldots,\lambda_q$ be the eigenvalues of the space–time matrix $\mathbf{\Psi}$. It is not difficult to prove $\lambda_i\neq\lambda_j$ for $\forall i,j\in\{1,\ldots,q\}$ with $i\neq j$; otherwise there exist $\lambda_k=\lambda_m$ with $k\neq m$, and this means that the $k$ th source and the $m$ th source have the same carrier frequency and angle of incidence, which is contradiction with assumption. Thus, no eigenvalue of $\mathbf{\Psi}$ is repeated, namely, the characteristic equation $f(\lambda)=\prod_{k=1}^{n}(\lambda-\lambda_k)$ $(\lambda_k\neq\lambda_m,\ k\neq m)$.

To prove that $f(\lambda)=m(\lambda)$, firstly, we prove $m(\lambda)$ divides $f(\lambda)$.

Because $\deg[m(\lambda)]\leq\deg[f(\lambda)]$ insures the existence of polynomials $q(\lambda)$ and $r(\lambda)$ (quotient and remainder) such that

$$f(\lambda)=m(\lambda)q(\lambda)+r(\lambda)\quad\text{where }\deg[r(\lambda)]<\deg[m(\lambda)]$$

Since

$$\mathbf{0}=f(\mathbf{\Psi})=m(\mathbf{\Psi})q(\mathbf{\Psi})+r(\mathbf{\Psi})=r(\mathbf{\Psi})$$

it follows that $r(\lambda)\equiv 0$; otherwise $r(\lambda)$, when normalized to be monic, would be annihilating polynomial having degree smaller than the degree of the minimum polynomial. So, the minimum polynomial $m(\lambda)$ divides the characteristic polynomial $f(\lambda)$.

Secondly, we prove that $f(\lambda)$ divides $m(\lambda)$.

Assume that $(\lambda_k,\mathbf{x}_k)$ is an eigenpair for $\mathbf{\Psi}$, then

$$\mathbf{\Psi}\mathbf{x}_k=\lambda_k\mathbf{x}_k\Rightarrow m(\mathbf{\Psi})\mathbf{x}_k=m(\lambda)_k\mathbf{x}_k$$
$$m(\mathbf{\Psi})=\mathbf{0}\Rightarrow m(\lambda_k)\mathbf{x}_k=\mathbf{0}\Rightarrow m(\lambda_k)=0 \tag{21}$$

Let $m(\lambda)=f(\lambda)q(\lambda)+r(\lambda)$, where $\deg[r(\lambda)]<\deg[f(\lambda)]=n$. From (21), it is clear that $r(\lambda)$ has $n$ distinct roots $(\lambda_1,\ldots,\lambda_n)$. However, $\deg[r(\lambda)]<n$, therefore, (21) holds if and only if $r(\lambda)\equiv 0$, namely, the characteristic polynomial $f(\lambda)$ divides the minimum polynomial $m(\lambda)$.

Finally, according to the Definitions 3.1 and 3.2, we can draw a conclusion that $f(\lambda)=m(\lambda)$. This concludes the proof.

## References


[1] M.A. Zatman, H.J. Strangeways, An efficient joint direction of arrival and frequency ML estimator, in: Proceedings of the IEEE Antennas and Propagation Society International Symposium, vol. 1, 1995, pp. 431–434.

[2] F. Atheley, Asymptotically decoupled angle–frequency estimation with sensor arrays, in: Proceedings of the IEEE Signals, Systems, and Computers, 1999, pp. 1098–1102.

[3] B.H. Fleury, M. Tschudin, et al., Channel parameter estimation in mobile radio environments using the SAGE algorithm, IEEE Journal on Selected Areas in Communications 17 (3) (1999) 434–450.

[4] R.O. Schmidt, Multiple emitter location and signal parameter estimation, in: Proceedings of the RADC Spectral Estimation Workshop, Rome, NY, 1979, pp. 243–258.

[5] S. Wang, J. Caffery, X. Zhou, Analysis of a joint space-time DOA/FOA estimator using MUSIC, in: Proceedings of the IEEE International Symposium on Personal, Indoor and Mobile Radio Communications, 2001, pp. B138–142.

[6] J.D. Lin, W.H. Fang, Y.Y. Wang, J.T. Chen, FSF MUSIC for joint DOA and frequency estimation and its performance analysis, IEEE Transactions on Signal Processing 54 (12) (2006) 4529–4542.

[7] R. Roy, T. Kailath, ESPRIT–estimation of signal parameters via rotational invariance techniques, IEEE Transactions on Acoustics, Speech, and Signal Processing 37 (7) (1989) 984–995.

[8] M. Haardt, M.D. Zoltowski, C.P. Mathcws, J.A. Nossek, 2D unitary ESPRIT for efficient 2D parameter estimation, in: Proceedings of the IEEE International Conference on Acoustic, Speech, Signal Processing, 1995, pp. 2096–2099.

[9] T. Kuroda, N. Kikuma, N. Inagaki, DOA estimation and pairing method in 2D-ESPRIT using triangular antenna array, Electrons and Communications in Japan 86 (6) (2003) 1505–1513.

[10] A.J. Van der Veen, P.B. Ober, E.F. Deprettere, Azimuth and elevation computation in high resolution DOA estimation, IEEE Transactions Signal Processing 40 (7) (1992) 1828–1832.

[11] F.L. Liu, J.K. Wang, R.Y. Du, G. Yu, Space-time matrix method for 2-D direction-of-arrival estimation, Signal Processing 87 (1) (2007) 101–106.

[12] M.C. Van der veen, A.J. Van der veen, A. Paulraj, Estimation of multipath parameters in wireless communications, IEEE Transactions on Signal Processing 46 (3) (1998) 682–690.

[13] A.J. Van der veen, M.C. Van der veen, A. Paulraj, Joint angle and delay estimation using shift-invariance techniques, IEEE Transactions on Signal Processing Letters (1997) 100–104.

[14] Y.Y. Wang, J.T. Chen, W.H. Fang, Joint estimation of the DOA and delay based on the TST-ESPRIT in wireless channel, in: IEEE Third Workshop on Signal Processing Advances in Wireless Communications, 2001, pp. 302–305.

[15] M.D. Zoltowski, C.P. Mathews, Real-time frequency and 2-D angle estimation with sub-Nyquist spatio-temporal sampling, IEEE Transactions on Signal Processing 42 (10) (1994) 2781–2794.

[16] M. Haardt, J.A. Nossek, 3-D unitary ESPRIT for joint angle and carrier estimation, in: Proceedings of the ICASSP, Munich, Germany, 1997, pp. 255–258.

[17] Y.H. Chen, C.H. Chen, Direction-of-arrival and frequency estimations for narrowband sources using two single rotation invariance algorithms with the marked subspace, in: Proceedings of the Institute of Electronic Engineering Radar Signal Processing, vol. 139, 1992, pp. 297–300.

[18] L. Ge, T. Chen, X. Huang, Simultaneous frequency and direction estimation from parallel-array data, in: Proceedings of the Institute of Electronic Engineering on Radar, Sonar, Navigation, vol. 142, no. 1, 1995, pp. 6–10.

[19] A.N. Lemma, A.J. van der Veen, E.F. Deprettere, Analysis of joint angle–frequency estimation using ESPRIT, IEEE Transactions on Signal Processing 51 (5) (2003) 1264–1283.

[20] A.N. Lemma, A.J. van der Veen, A. Paulraj, Joint angle–frequency estimation using multi-resolution ESPRIT, in: Proceedings of the ICASSP, Seattle, WA, 1998, pp. 1957–1960.

[21] M. Haardt, J.A. Nossek, Unitary ESPRIT: how to obtain increased estimation accuracy with a reduced computational burden, IEEE Transactions on Signal Processing 43 (5) (1995) 1232–1242.

[22] M. Zoltowski, M. Haardt, C.P. Mathcws, Closed-form 2-D angle estimation with rectangular arrays in element space or beamspace via Unitary ESPRIT, IEEE Transactions on Signal Processing 44 (2) (1996) 316–328.

[23] A.J. van der Veen, A. Paulraj, An analytical constant modulus algorithm, IEEE Transactions on Signal Processing 44 (5) (1996) 1136–1155.

[24] L.D. Lathauwer, Signal processing based on multilinear algebra, Ph.D. Dissertation, Katholieke University, Leuven, Belgium, 1997.

[25] T.J. Shan, M. Wax, T. Kailath, On spatial smoothing for direction-of-arrival estimation of coherent signals, IEEE Transactions on Acoustics, Speech, Signal Processing (ASSP-33) (1985) 806–811.

[26] M. Wax, T. Kailath, Detection of signal by information theoretic criteria, IEEE Transactions on Acoustics, Speech, Signal Processing (33) (1985) 387–392.

[27] J. Hefferon, Linear algebra 〈http://joshua.smcvt.edu/linalg.html/〉.

[28] K.Y. Zhang, Z. Xu, Numerical Algebra, Science Press, Beijing, 2000.

[29] D.F. Han, Q.B. Wu, Numerical Computing Methods, Zhejiang University Press, 2002.

[30] J.D. Lin, W.H. Fang, K.H. Wu, J.T. Chen, FSF subspace-based algorithm for joint DOA-FDOA estimation, in: Proceedings of the IEEE International Conference on Acoustics, Speech, Signal Processing, 2004, pp. 157–160.

[31] P. Stoica, A. Nehorai, Performance study of conditional and unconditional direction-of-arrival estimation, IEEE Transactions on Acoustics, Speech, Signal Processing 38 (10) (1990) 1783–1795.

[32] G.G. Raleigh, T. Boros, Joint space–time parameter estimation for wireless communication channels, IEEE Transactions on Signal Processing 46 (5) (1998) 1333–1343.